Supplementary Information

Defect engineering and triangular copper as key drivers for ultralow thermal conductivity in Cu_2ZrS_3 polytypes

Lucas Le Gars,[1,*] Sakshi Verma,[2] Minati Tiadi,[1] Carmelo Prestipino,[1,*] Animesh Das,[2] Bin Zhang,[3,4] Olivier Perez,[1] Philippe Boullay,[1] Denis Menut,[5] Bernard Raveau,[1] Gaëlle Riou,[1] Adèle Renaud,[6] Kanishka Biswas,[2] Umesh V. Waghmare,[2] Xiaoyuan Zhou,[3,4] Koichiro Suekuni,[7] and Emmanuel Guilmeau[1,*]

[1] *CRISMAT, CNRS, Normandie Univ, ENSICAEN, Unicaen, 14000 Caen, France*

[2] *Jawaharlal Nehru Centre for Advanced Scientific Research (JNCASR), Jakkur, Bengaluru, Karnataka - India*

[3] *College of Physics and Institute of Advanced Interdisciplinary Studies, Chongqing University, Chongqing 401331, China*

[4] *Analytical and Testing Center of Chongqing University, Chongqing 401331, China*

[5] *Ligne MARS, L'Orme des Merisiers, Synchrotron SOLEIL, 91192 Saint-Aubin, Gif-sur-Yvette, France*

[6] *Univ. Rennes, CNRS, ISCR – UMR 6226, F-35000 Rennes, France*

[7] *Interdisciplinary Graduate School of Engineering Sciences, Kyushu University, 6–1 Kasugakouen, Kasuga, Fukuoka 816–8580, Japan*

Contact authors: lucas.le-gars@ensicaen.fr; carmelo.prestipino@ensicaen.fr;

emmanuel.guilmeau@ensicaen.fr

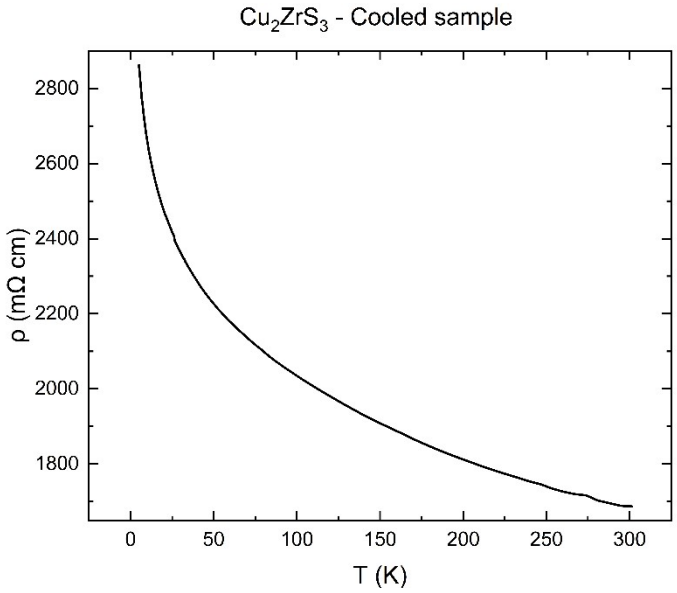

Figure S1. Measurement of the resistivity of Cu_2ZrS_3 at low temperature.

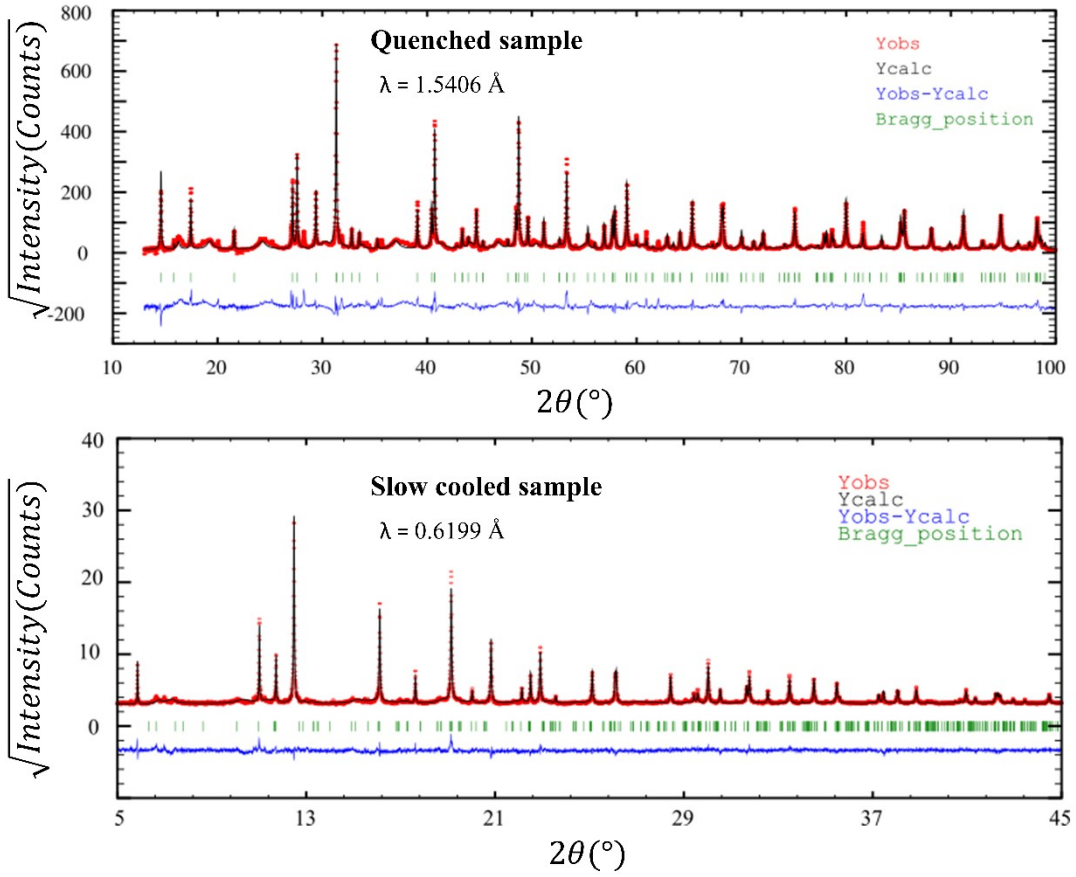

Figure S2. Rietveld refinement of synchrotron XRD patterns of a) quenched sample and b) slow cooled sample, considering stacking fault models.

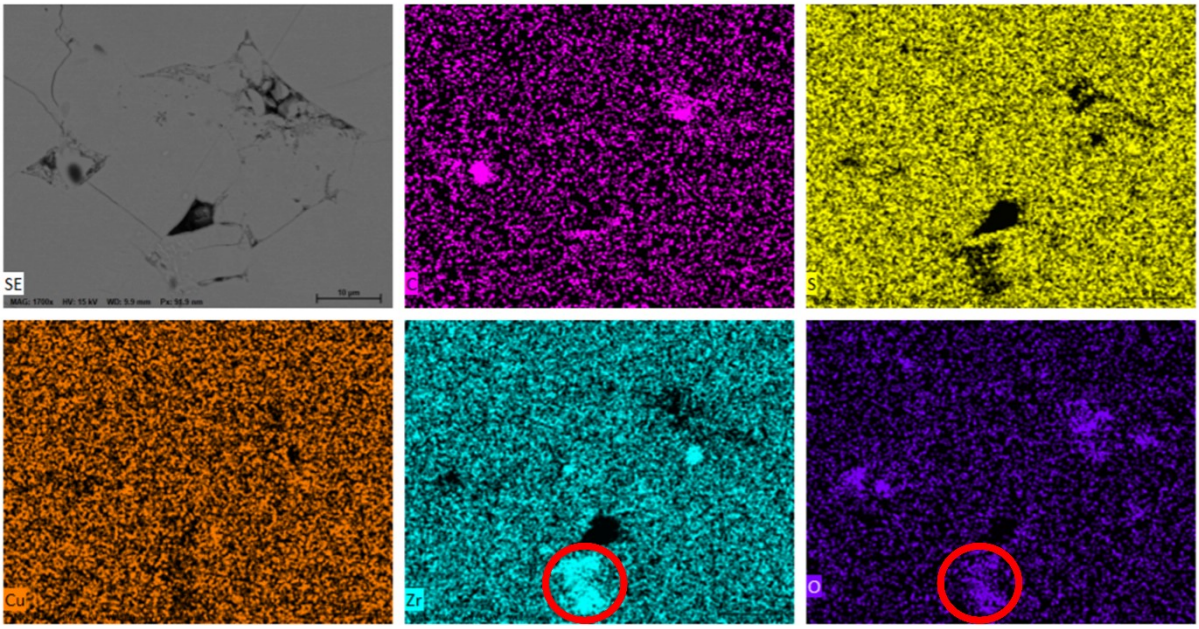

Figure S3. EDX mapping of the slow-cooled Cu_2ZrS_3 sample.

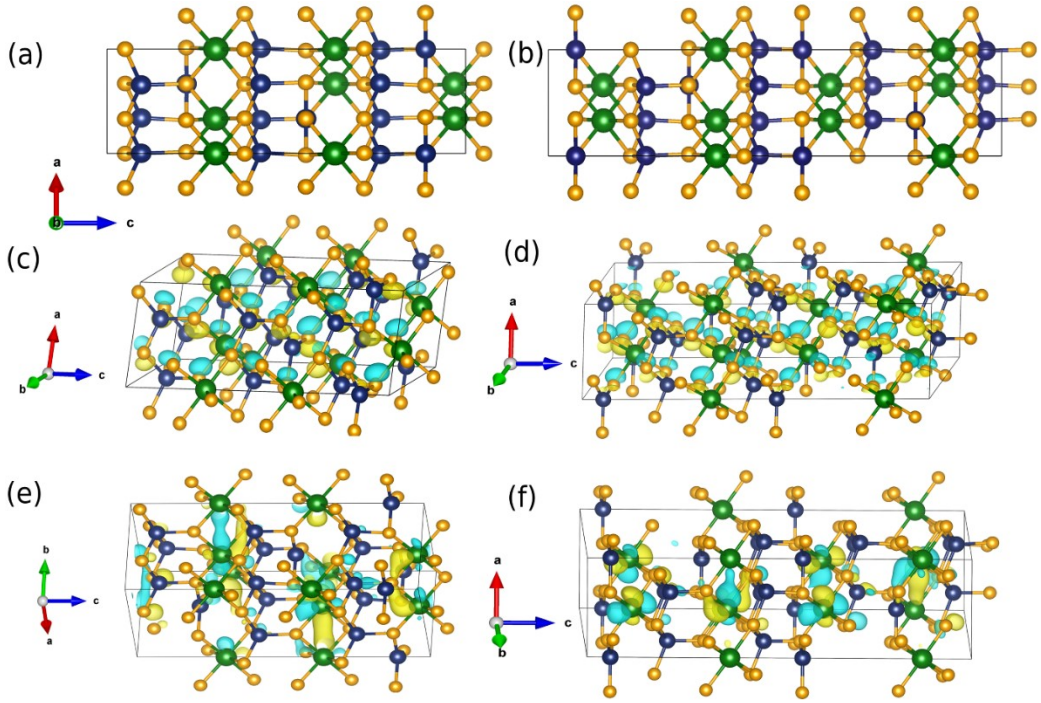

Figure S4. Crystal structures and visualization of wavefunctions at band edges of Cu_2ZrS_3. Optimized structures obtained with ABC (a) and ABCB (b) stacking of its layers. Spheres in green, blue and orange represent Zr, Cu and S respectively. Cu atoms coordinated with three S form a planar structure with them. Visualization of wavefunctions at VBM shows S-*p* orbitals

for ABC (c) and ABCB (d) stackings respectively and that at CBM reveals Zr-*d* orbitals as well as interactions between Zr-Zr and Zr-S (e) and (f)

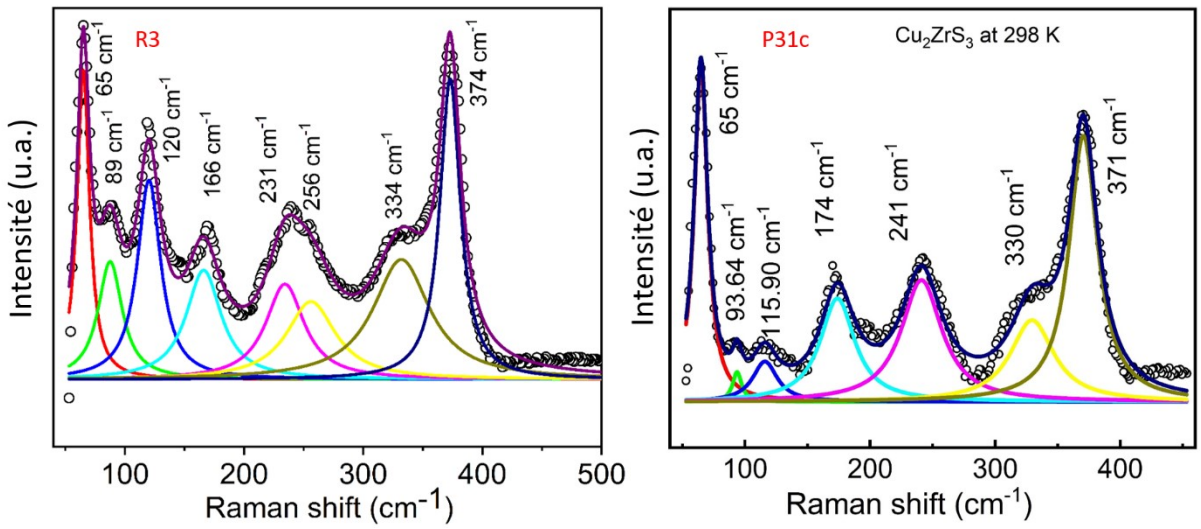

Figure S5. Room temperature Raman spectra of Cu_2ZrS_3 in *R*3 space group.

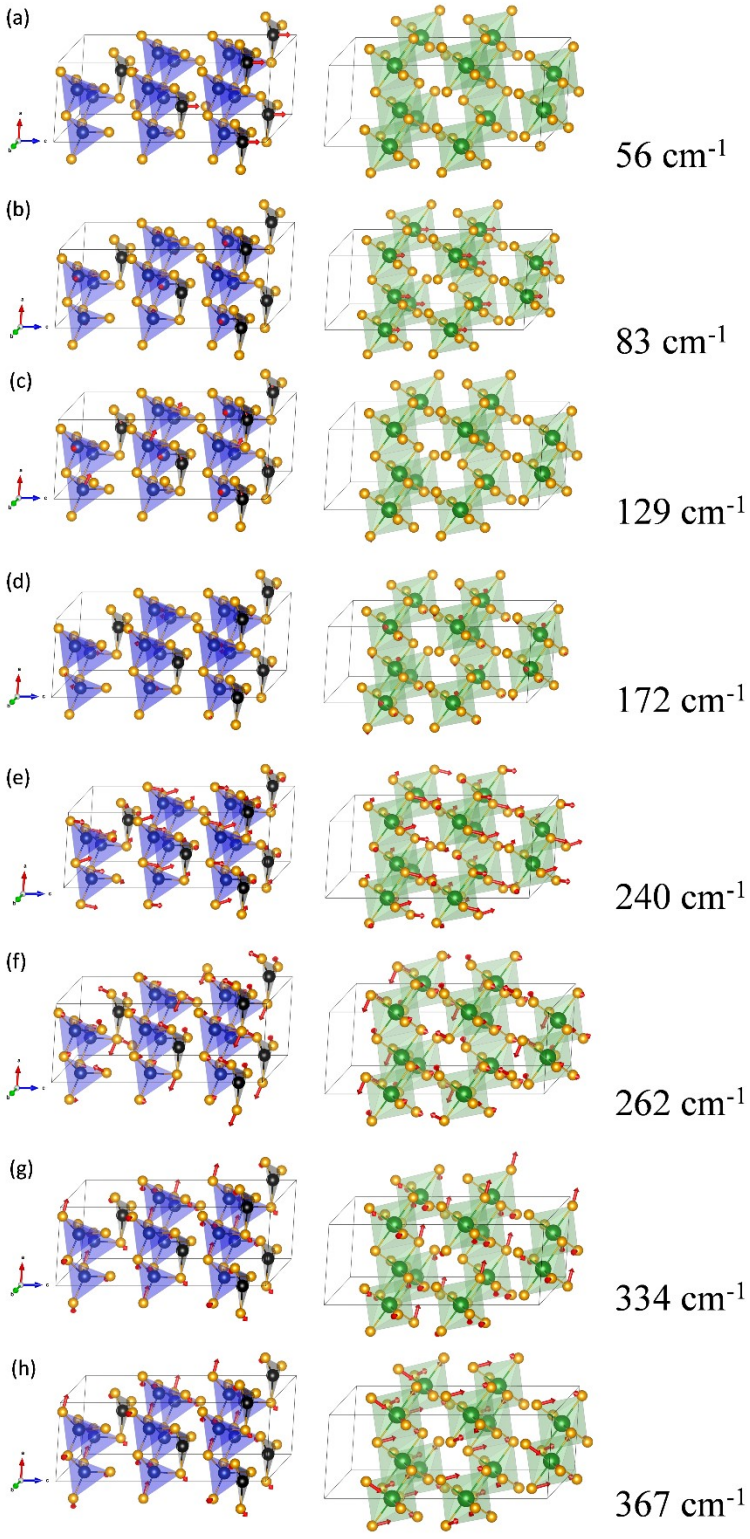

Figure S6. Visualization of the Raman active modes of R3 phase (ABC stacking) at frequencies 56 cm^{-1}, 83 cm^{-1}, 129 cm^{-1}, 172 cm^{-1}, 240 cm^{-1}, 262 cm^{-1}, 334 cm^{-1} and 367 cm^{-1} shown in (a)-(h) respectively. Spheres in green, blue, black and yellow colors denote Zr, Cu in four fold coordination, Cu in three fold coordination and S respectively. For ease of visualization, the Cu and Zr sublattices are shown separately.

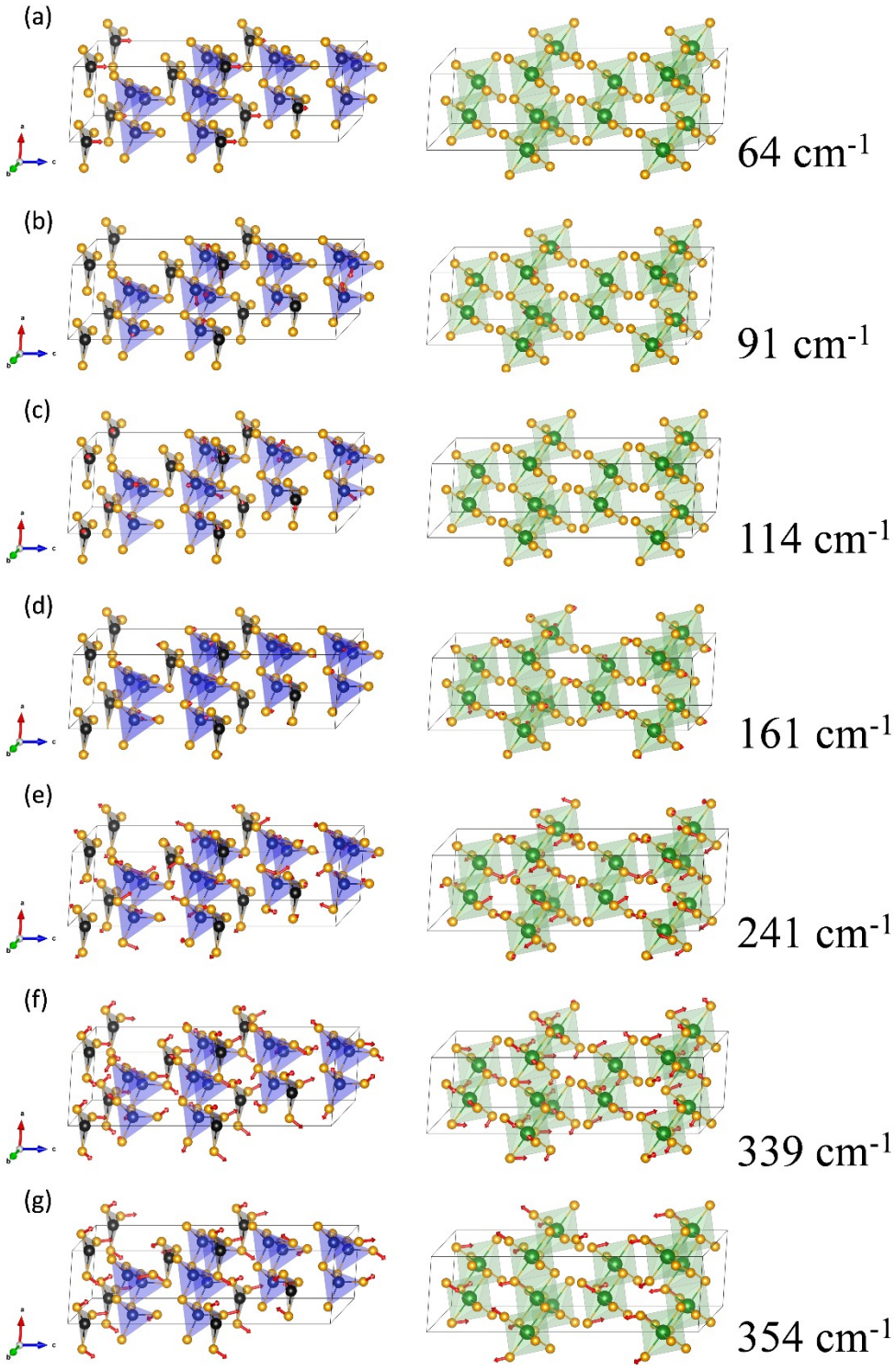

Figure S7. Visualization of the Raman active modes of P31*c* phase (ABCB stacking) at frequencies 64 cm^{-1}, 91 cm^{-1}, 114 cm^{-1}, 161 cm^{-1}, 241 cm^{-1}, 339 cm^{-1} and 354 cm^{-1} shown in (a)-(g) respectively. Spheres in green, blue, black and yellow colors denote Zr, Cu in four fold coordination, Cu in three fold coordination and S respectively. For ease of visualization, the Cu and Zr sublattices are shown separately.

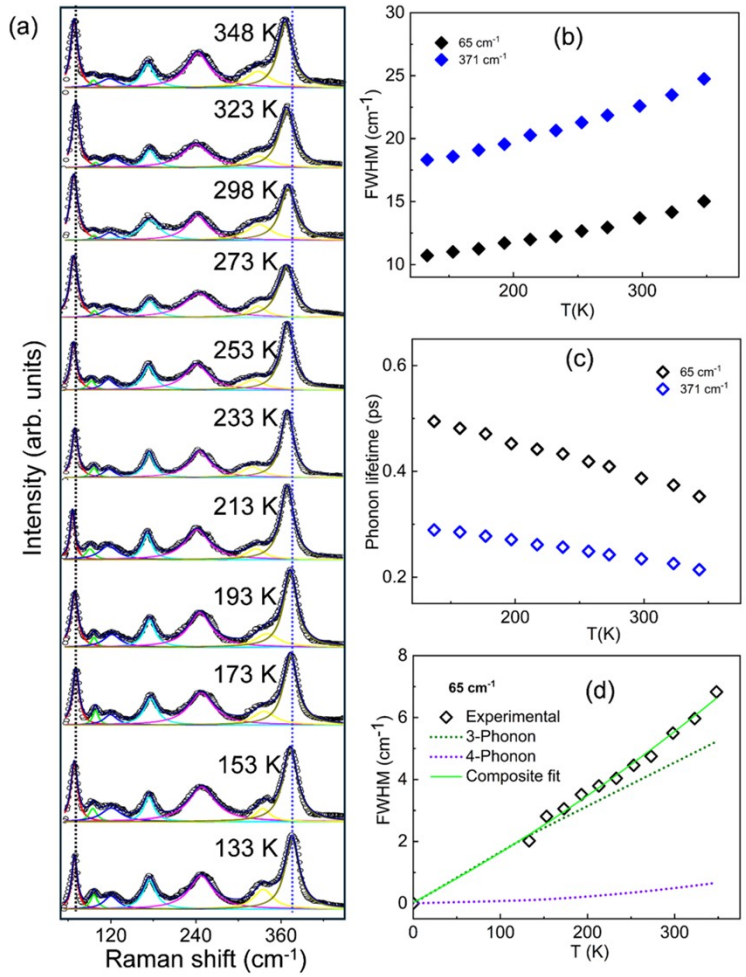

Figure S8. (a) Temperature-dependent Raman spectra of the P31*c* Cu_2ZrS_3 compound measured from 133 to 348 K. (b) Full width at half maximum (FWHM) of the Raman modes at 65, and 371 cm^{-1} as a function of temperature. (c) Calculated phonon lifetimes corresponding to the 65 and 371 cm^{-1} Raman modes. (d) Decomposition of the FWHM of the 65 cm^{-1} Raman mode into anharmonic contributions from three-phonon and four-phonon scattering processes in Cu_2ZrS_3.

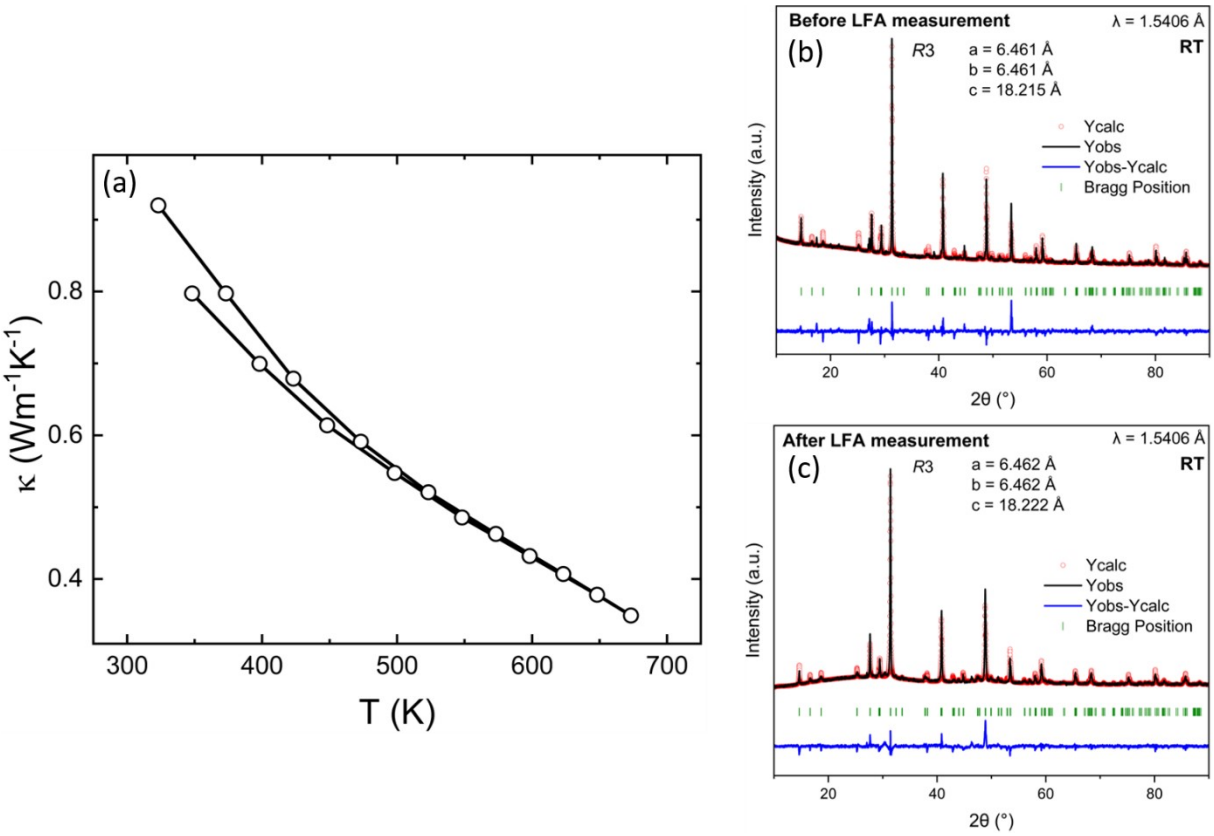

Figure S9. (a) Thermal conductivity of the slowly-cooled Cu_2ZrS_3 sample and XRD patterns (b) before and (c) after LFA measurement, confirming *R3* phase stability.

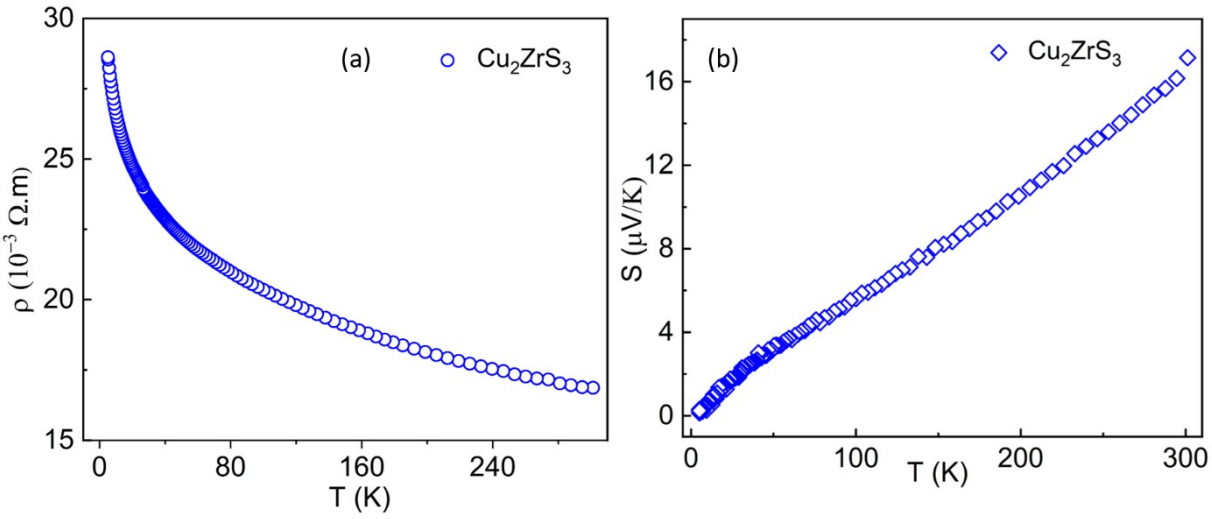

Figure S10. Temperature-dependent (a) electrical conductivity (ρ), (b) Seebeck coefficient (*S*) of Cu_2ZrS_3 sample measured from 5 K to 300 K

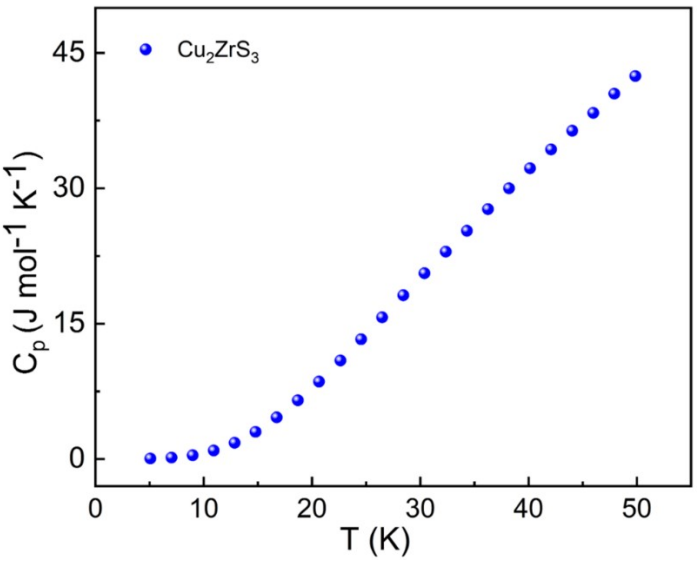

Figure S11. Low temperature (5-49 K) heat capacity (C_P) of Cu_2ZrS_3

$$v_S = \left(\frac{1}{3}\left[\frac{1}{{v_L}^3} + \frac{2}{{v_T}^3}\right]\right)^{-1/3}$$

$$v_p = \frac{1 - 2\left(\frac{v_T}{v_L}\right)^2}{2 - 2\left(\frac{v_T}{v_L}\right)^2}, \quad \Upsilon = \frac{3}{2}\left(\frac{1 + v_p}{2 - 3v_p}\right)$$

Equations S1. Expressions used to calculate the average sound velocity v_S, the Poisson's ratio v_p, and the Grüneisen parameter γ from the longitudinal (v_L) and transverse (v_T) sound velocities.

Table S1. Quench sample, structural parameters obtained from single crystal X-ray diffraction. Fractional atomic coordinates, equivalent isotropic displacement parameters, and anisotropic displacement parameter (Å^2).

Cu_2ZrS_3 Trigonal, P31*c* Temperature (K): 293 *a* = 6.47548 (15), *c* = 24.3290 (5) (Å), V=883.48 (3) (Å^3), Z=6 No. of measured (47270,), independent (21731) and observed [I > 3σ(I)] reflections (11070) R_{int} =3.3 %, R[F^2 > 2σ(F^2)] = 0.074, wR(F^2) = 0.240, S= 1.30					
	x	*y*	*z*	U_{eq} (Å^2)	Occ. (<1)
Zr1	0	0	0.37070 (8)	0.00949 (8)	
Zr2	⅔	⅓	0.62157 (10)	0.00865 (12)	
Zr3	⅓	⅔	0.61960 (10)	0.00951 (12)	
Zr4/Cu1	⅓	⅔	0.37058 (5)	0.00903 (9)	0.5/0.5
Zr5/Cu2	0.66125 (6)	0.99671 (6)	0.21592 (7)	0.01484 (15)	0.083/0.917
Zr6/Cu3	0.00456 (6)	0.66845 (6)	0.46591 (7)	0.01487 (15)	0.083/0.917
Cu4	0	0	0.56406 (11)	0.0259 (2)	
Cu5	⅔	⅓	0.31403 (5)	0.0287 (2)	
S1	0.66754 (12)	0.98703 (14)	0.31083 (9)	0.0097 (3)	
S2	0.99879 (13)	0.65112 (16)	0.56073 (11)	0.0096 (3)	
S3	0.33721 (12)	0.00246 (11)	0.18026 (11)	0.0084 (3)	
S4	0.32985 (12)	0.99786 (11)	0.43034 (9)	0.0082 (3)	

	U_{11}	U_{22}	U_{33}	U_{12}	U_{13}	U_{23}
Zr1	0.00801 (10)	U_{11}	0.01244 (16)	½ U_{11}	0	0
Zr2	0.00824 (13)	U_{11}	0.0095 (3)	½ U_{11}	0	0
Zr3	0.00837 (13)	U_{11}	0.0118 (2)	½ U_{11}	0	0
Zr4/Cu1	0.00848 (11)	U_{11}	0.01014 (16)	½ U_{11}	0	0
Zr5/Cu2	0.01711 (18)	0.0197 (2)	0.0089 (2)	0.01014 (13)	−0.00169 (10)	−0.00056 (9)
Zr6/Cu3	0.01760 (19)	0.01707 (19)	0.0087 (2)	0.00774 (12)	0.00147 (9)	0.00126 (11)
Cu4	0.0213 (2)	U_{11}	0.0349 (4)	½ U_{11}	0	0
Cu5	0.0242 (3)	U_{11}	0.0377 (5)	½ U_{11}	0	0
S1	0.0084 (3)	0.0124 (3)	0.0074 (5)	0.0045 (2)	−0.0007 (2)	0.0018 (3)

S2	0.0080 (3)	0.0126 (3)	0.0076 (5)	0.0047 (2)	0.00100 (17)	0.0022 (3)
S3	0.0087 (3)	0.0079 (3)	0.0086 (6)	0.0041 (2)	0.00215 (19)	−0.00054 (18)
S4	0.0092 (3)	0.0091 (4)	0.0073 (6)	0.0052 (2)	−0.00187 (18)	−0.00199 (18)

Table S2. Slow cooled sample, structural parameters obtained from single crystal X-ray diffraction. Fractional atomic coordinates, equivalent isotropic displacement parameters, and anisotropic displacement parameter (Å^2).

Cu_2ZrS_3 Trigonal, R3 Temperature (K): 150 a = 6.4573(2), c = 18.1755 (6) (Å), V=656.3148 (Å^3) Z=6 No. of measured (1750), independent (721) and observed [I > 3σ(I)] reflections (721) R_{int} =2.1%, R[F^2 > 2σ(F^2)] = 0.052, wR(F^2) = 0.156, S= 3.75				
	x	y	z	U_{eq} (Å^2)
Cu1	−0.3358 (2)	−0.3361 (2)	0.0975 (2)	0.0083 (8)
Cu2	0	0	−0.10625 (17)	0.0195 (10)
S1	0.0074 (5)	−0.6651 (5)	0.2226 (3)	0.0065 (9)
S2	−0.3322 (5)	0.0017 (5)	0.0496 (4)	0.0044 (10)
Zr1	0	0	0.30400 (9)	0.0045 (6)
Zr2	0	0	0.63509 (9)	0.0048 (6)

	U_{11}	U_{22}	U_{33}	U_{12}	U_{13}	U_{23}
Cu1	0.0084 (10)	0.0093 (10)	0.0065 (10)	0.0039 (6)	−0.0008 (5)	−0.0018 (5)
Cu2	0.0206 (12)	U_{11}	0.0174 (16)	½ U_{11}	0	0
Zr1	0.0048 (7)	U_{11}	0.0037 (9)	½ U_{11}	0	0
Zr2	0.0025 (7)	U_{11}	0.0094 (12)	½ U_{11}	0	0

Table S3. Slow cooled sample, structural parameters obtained from precession-assisted 3D ED (dynamical refinement). Fractional atomic coordinates, equivalent isotropic displacement parameters, and anisotropic displacement parameter (Å^2).

Cu_2ZrS_3 Trigonal, R3 Temperature (K): 297 a = 6.6489 (13), c = 18.753 (4) (Å), V = 718 (Å^3), Z=6 R(obs) = 0.087, R(all) = 0.087, wR(all) = 0.212, GoF(obs)= 6.16 No. of measured (10830), independent (4207) and observed [I > 3σ(I)] reflections (4180) Dynamical refinement parameters: g_{max} (Å^{-1})=1.6, Sg_{max} (Å^{-1})=0.01, RSg_{max}=0.66, steps=128				
	x	y	z	U_{eq} (Å^2)
Zr1	⅓	⅔	0.52780 (15)	0.0073 (6)
Zr2	0	0	0.53*	0.0086 (6)
Cu1	0.0066 (2)	0.3381 (2)	0.40133 (18)	0.0147 (6)
Cu2	⅔	⅓	0.6035 (2)	0.0212 (10)
S1	0.3184 (4)	−0.0175 (4)	0.6098 (2)	0.0099 (9)
S2	0.3295 (3)	0.3316 (3)	0.44916 (19)	0.0061 (8)

	U_{11}	U_{22}	U_{33}	U_{12}	U_{13}	U_{23}
Zr1	0.0059 (5)	U_{11}	0.0101 (15)	½ U_{11}	0	0
Zr2	0.0071 (5)	U_{11}	0.0116 (16)	½ U_{11}	0	0
Cu1	0.0182 (6)	0.0207 (6)	0.0059 (11)	0.0103 (5)	−0.0016 (6)	−0.0007 (6)
Cu2	0.0201 (7)	U_{11}	0.024 (3)	½ U_{11}	0	0
S1	0.0130 (9)	0.0115 (9)	0.0088 (17)	0.0088 (8)	−0.0029 (11)	−0.0023 (10)
S2	0.0084 (8)	0.0076 (8)	0.0022 (18)	0.0039 (7)	0.0022 (9)	0.0017 (10)

** fixed parameter*

Table S4. Calculated Formation Energies of Cu_2ZrS_3 for Different Stacking Sequences

Stacking	**Space group**	**Energy eV / f.u.**
AB	P31*c*	+ 0.0001(30)
ABC	R3	0

ABCB	P31*c*	+ 0.0003(30)

Table S5. Calculated fitting parameters from the Klemens model for Cu_2ZrS_3 in the temperature range 77-343 K.

Modes Raman		**3-phonon constant (A) in cm^{-1}**	**4-phonon constant (B) in cm^{-1}**
R3	65 cm^{-1}	0.30	0.0018
	166 cm^{-1}	0.90	0.028
P31*c*	65 cm^{-1}	0.27	0.0023
	371 cm^{-1}	0.86	0.031

Table S6. Parameters obtained from the fitting of low-temperature Cp/T vs. T^2 data of Cu_2ZrS_3 using Debye-Einstein model with three Einstein oscillators.

Parameters	**Values**
γ	0.0078
β	5.06478E-5
Θ_{E1}(K)	50.83 (35.27 cm^{-1})
Θ_{E2}(K)	95.68 (66.38 cm^{-1})
Θ_{E3} (K)	156.47 (108.56 cm^{-1})
Θ_D(K)	285.85
A1	2.180
A2	27.324
A3	28.882
R2	0.999
χ^2	1.0675E-6

Table S7. Debye-Callaway model fitted parameter of Cu_2ZrS_3 in the R3 polytype.

Parameter of Cu_2ZrS_3	**Value**
m	6.20
L (μm)	0.28
A	3.42×10^{-42}
B	4.93×10^{-17}
Sound velocity (m/s)	1971
Debye temperature (K)	285

References

(1) Petříček, V.; Dušek, M.; Palatinus, L. Crystallographic Computing System JANA2006: General Features. *Z. Für Krist. - Cryst. Mater.* **2014**, *229* (5), 345–352. https://doi.org/10.1515/zkri-2014-1737.

(2) Palatinus, L.; Chapuis, G. *SUPERFLIP* – a Computer Program for the Solution of Crystal Structures by Charge Flipping in Arbitrary Dimensions. *J. Appl. Crystallogr.* **2007**, *40* (4), 786–790. https://doi.org/10.1107/S0021889807029238.

(3) Sitaud, B.; Solari, P. L.; Schlutig, S.; Llorens, I.; Hermange, H. Characterization of Radioactive Materials Using the MARS Beamline at the Synchrotron SOLEIL. *J. Nucl. Mater.* **2012**, *425* (1–3), 238–243. https://doi.org/10.1016/j.jnucmat.2011.08.017.

(4) Rodríguez-Carvajal, J. Recent Advances in Magnetic Structure Determination by Neutron Powder Diffraction. *Phys. B Condens. Matter* **1993**, *192* (1–2), 55–69. https://doi.org/10.1016/0921-4526(93)90108-I.

(5) Roisnel, T. WiinPLOTR, a Graphic Tool for Powder Diffraction. *Mater. Sci. Forum* **2001**, *378*.

(6) Casas-Cabanas, M.; Reynaud, M.; Rikarte, J.; Horbach, P.; Rodríguez-Carvajal, J. *FAULTS* : A Program for Refinement of Structures with Extended Defects. *J. Appl. Crystallogr.* **2016**, *49* (6), 2259–2269. https://doi.org/10.1107/S1600576716014473.

(7) Alleno, E.; Bérardan, D.; Byl, C.; Candolfi, C.; Daou, R.; Decourt, R.; Guilmeau, E.; Hébert, S.; Hejtmanek, J.; Lenoir, B.; Masschelein, P.; Ohorodnichuk, V.; Pollet, M.; Populoh, S.; Ravot, D.; Rouleau, O.; Soulier, M. Invited Article: A Round Robin Test of the Uncertainty on the Measurement of the Thermoelectric Dimensionless Figure of Merit of $Co_{0.97}Ni_{0.03}Sb_3$. *Rev. Sci. Instrum.* **2015**, *86* (1), 011301. https://doi.org/10.1063/1.4905250.

(8) Kresse, G.; Hafner, J. *Ab Initio* Molecular Dynamics for Liquid Metals. *Phys. Rev. B* **1993**, *47* (1), 558–561. https://doi.org/10.1103/PhysRevB.47.558.

(9) Kresse, G.; Furthmüller, J. Efficiency of Ab-Initio Total Energy Calculations for Metals and Semiconductors Using a Plane-Wave Basis Set. *Comput. Mater. Sci.* **1996**, *6* (1), 15–50. https://doi.org/10.1016/0927-0256(96)00008-0.

(10) Kresse, G.; Furthmüller, J. Efficient Iterative Schemes for *Ab Initio* Total-Energy Calculations Using a Plane-Wave Basis Set. *Phys. Rev. B* **1996**, *54* (16), 11169–11186. https://doi.org/10.1103/PhysRevB.54.11169.

(11) Perdew, J. P.; Ruzsinszky, A.; Csonka, G. I.; Vydrov, O. A.; Scuseria, G. E.; Constantin, L. A.; Zhou, X.; Burke, K. Restoring the Density-Gradient Expansion for Exchange in Solids and Surfaces. *Phys. Rev. Lett.* **2008**, *100* (13), 136406. https://doi.org/10.1103/PhysRevLett.100.136406.

(12) Togo, A.; Chaput, L.; Tadano, T.; Tanaka, I. Implementation Strategies in Phonopy and Phono3py. *J. Phys. Condens. Matter* **2023**, *35* (35), 353001. https://doi.org/10.1088/1361-648X/acd831.

(13) Togo, A. First-Principles Phonon Calculations with Phonopy and Phono3py. *J. Phys. Soc. Jpn.* **2023**, *92* (1), 012001. https://doi.org/10.7566/JPSJ.92.012001.